Theoretical Chemistry Accounts (2023) 142:107
https://doi.org/10.1007/s00214-023-03038-0

RESEARCH

A computational study of two promising tweezers

Mohammad Sayaheen[1] · Nicolás Otero[1] · Angeles Peña-Gallego[1]

Received: 6 May 2023 / Accepted: 22 August 2023 / Published online: 1 October 2023

Abstract
A DFT study was carried out to explore the properties of two nonplanar π-conjugated systems that share dibenzo[a,e]-cyclooctatetraene (DBCOT) as a fundamental element. These systems were presented as molecules with potential use as tweezers and in optoelectronic applications due to their expected nonlinear optical effects. Structure optimizations, TD-DFT calculations, molecular orbitals and topological analysis were performed for $C_{36}N_2H_{18}O_4$ and $C_{26}H_{18}$ structures, formed by one and two **1,3,5,7-**cyclooctatetraene rings, respectively, with and without the Na cation. This alkali cation was used as a model to investigate the potential of these molecules as tweezers. The results show a V-shaped structure as a minimum in the ground state for both molecules. This angular structure can trap the Na cation very effectively, especially for one of the cases. In addition, the present analysis opens new studies to explore the use of these systems as tweezers of other cations, anions or aromatic molecules that may exhibit π-stacking. The analysis of the molecular orbitals involved in the main electronic transitions allows us to propose that these systems will have interesting optical properties.

Keywords Nonplanar π-conjugated · Tweezers · NLO effects · Topological study

1 Introduction

In recent years, the study of nonplanar π-conjugated systems has reached a great development. These systems are expected to have important applications in fields, such as molecular electronics, solar cells, optoelectronic applications or sensing materials.

Several different structures have been proposed, ranging from corannulene [1] or cyclooctatetraene [2] to expanded porphyrins [3] or twisted perylene bisimides [4]. The size and shape of these structures play a fundamental role in achieving specific optical and electronic properties. Yamaguchi et al. [5] have pointed out the advantages of π-conjugated systems, which combine flexibility and rigidity. Among all these systems, we have had a closer look at two systems that are characterized by a combination of flexibility and rigidity, to be constituted by a flexible central part joining two rigid wings. The flexible unit gives rise to a dynamic conformational change in the excited state, from a nonplanar V-shaped structure to a planar structure. These systems, shown in Fig. 1, can also function as molecular tweezers, picking up other molecules.

The concept of molecular tweezers was first employed by Whitlock in 1978 [6] to name a caffeine-based receptor. A molecular tweezer was defined as a receptor in which two flat arms, usually aromatic, are separated by a rigid spacer. This spacer provides a suitable distance between the flat arms for the inclusion of an aromatic guest molecule through π–π interactions (around 7 Å).

In this study, we worked with two types of tweezers with different nonplanar bending schemes and their planar counterparts. On the one hand, tweezer one (tw1) ($C_{36}N_2H_{18}O_4$), synthesized by Yamaguchi et al. [5] is composed of a cyclooctatetraene ring in the center attached by three benzene rings and a pyrrolidine-2,5-dione on each side of the tweezer, as can be observed in Fig. 1A, C. On the other hand, tweezer two (tw2) ($C_{26}H_{18}$), based on proposed in previous works [7, 8], is formed by two cyclooctatetraene rings within three benzene rings, whose optimized angular and planar geometries, minimum and transition state in S0 electronic state, respectively, are shown in Fig. 1B, D, respectively. In addition, Fig. 1 includes vertical and front views of the angular and planar structures, respectively.

✉ Nicolás Otero
nom05@uvigo.es

✉ Angeles Peña-Gallego
mpena@uvigo.es

[1] Departamento de Química Física, Universidade de Vigo, 36310 Vigo, Spain

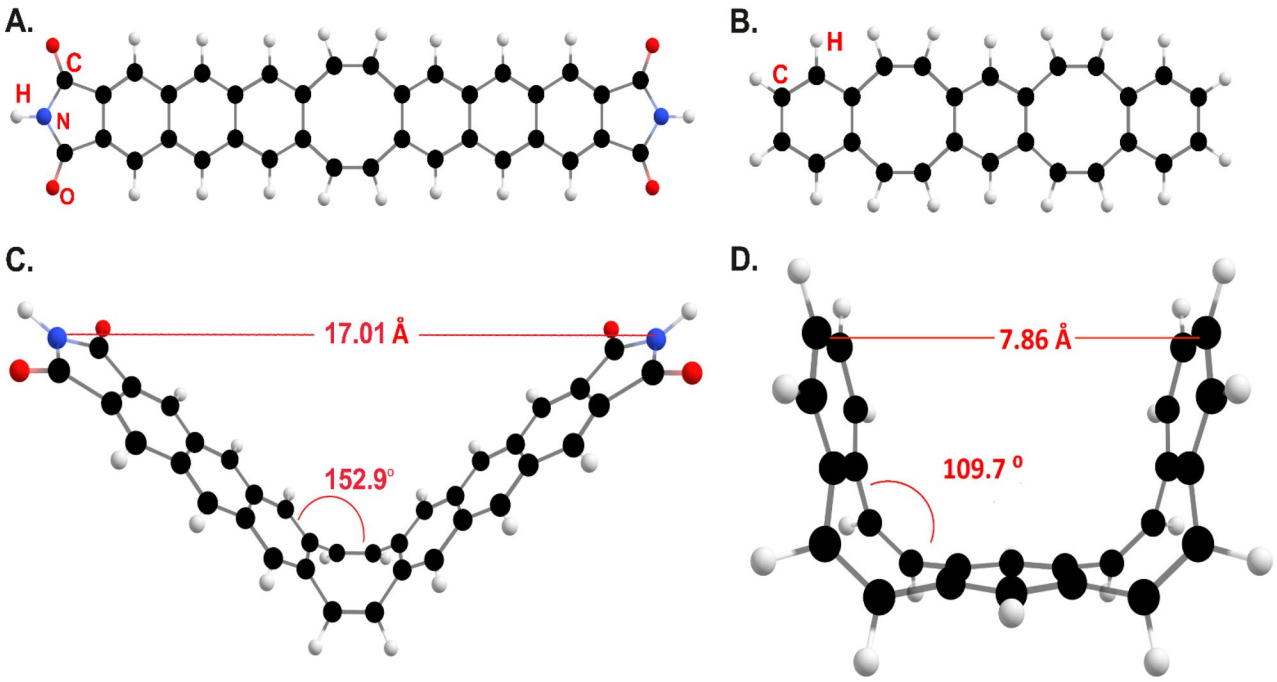

Fig. 1 Schematic representation of the structures tweezer one (**tw1**) (**A**, **C**) and tweezer two (**tw2**) (**B**, **D**), in both angular and planar conformations in the S0 electronic state. All carbon and hydrogen atoms are represented in black and white, respectively, while the oxygen (nitrogen) atoms are colored in red (blue). In the case of the angular structures, the angles were calculated via multilinear regression, as well as the maximum distance in Å between the heavy atoms of the tweezer arms are also included

We have conducted a computational study to analyze the suitability of these tweezers for use with cations, taking Na cation as a model. With this objective, not only a structural study of the systems with and without cation was performed, but also a topological analysis and interaction energies, which had not been done previously and which we consider essential to explore the feasibility of these systems as tweezers.

2 Computational details

All the tweezers' structures were fully optimized at the levels of B3LYP [9], CAM-B3LYP [10], M062X [11], MN12L [12], MN12SX [13], and ωB97X-D [14] density functional theories with two different Pople basis sets, 6-31G(d,p) and 6-31G(2d,2p). Initially for this work we considered the use of fuzzy functions through the 6-31++G(d,p) basis set, but no general improvements in their electronic properties were observed in many of the structures and, in addition, several of them suffered from SCF instabilities that did not allow us to consider them. The optimizations, wave function stability and geometry characterization with frequencies calculations were performed with Gaussian 09 [15]. TD-DFT calculations [16–18] were performed with Gaussian 16 [19], keeping the same mentioned functionals but using only with the 6-31G(d,p) basis set.

The angle of all nonplanar structures (Θ) was measured using a home-made Fortran program designed to calculate the angle between two estimated planes by means of multilinear regression techniques. In this way, we do not consider the dihedral angle of four atoms uniquely but an estimation of the real angle between two planes constituted by a larger set of atoms from two different planes, a more realistic way to study the planarity distortion.

A topological and charge analysis of the electron density, $\rho(\boldsymbol{r})$, at CAM-B3LYP/6-31G(d,p) was performed using the quantum theory of atoms in molecules (QTAIM) approach [20] for both tweezers with and without Na cation. Moreover, these populations have been compared with other real space partitioning based on the Hirshfeld idea of *fuzzy* atoms, called fractional occupation Hirshfeld-Iterative (FOHI) [21], where an iterative promolecular density is obtained by atomic SCF calculations optimizing the occupation numbers. The atomic charge of an unspecific atom A was computed as the difference between the nuclear charge $Z(A)$ and the corresponding integrated atomic population $N(A)$:

$$q(A) = Z(A) - N(A) \tag{1}$$

where $N(A)$ corresponds to the integral of a molecular region representing the atom A defined by the following expression:

$$N(A) = \int w_A(r)\rho(r)\mathrm{d}r \tag{2}$$

In the case of the QTAIM approach, the weight function, w_A, is equal to 1 if $w_A \in \Omega_A$, i.e., if w_A belongs to the atomic basin (Ω) of A. In the case of the Hirshfeld-based partitionings, in contrast with the discrete QTAIM definition, w_A belongs to the entire molecular space and is expressed as:

$$w_A(r) = \frac{\rho_A(r)}{\sum_{n=1}^{NAT} \rho_n(r)} \tag{3}$$

where NAT is the total number of atoms, and ρ_A and ρ_n stand for the proatomic densities obtained by the FOHI approach for the atom A and the atom n, respectively. Both intramolecular and intermolecular critical points (CPs), the corresponding bond paths, together with the value of the Laplacian of $\rho(\boldsymbol{r})$ ($\nabla^2\rho_b$), the gradient kinetic density ($G(\boldsymbol{r}_b)$), the virial field ($V(\boldsymbol{r}_b)$), and the ratio of the two previous energy densities at the bond critical points (BCPs) were computed using the AIMAll software package [22]. The accuracy achieved in the calculation of the QTAIM atomic properties was verified. Thus, the sums over the $q(\Omega)$ and the atomic energy values for each molecule reproduce the total charge and molecular electronic energies to within 1.7×10^{-3} au and 1.70 kJ mol^{-1}, respectively. All atoms were integrated with an absolute value of the integrated Laplacian function ($L(\Omega)$) less than 4.95×10^{-3} au. The sum over all absolute values of the atomic $L(\Omega)$ was less than 1.28×10^{-3} au. For the FOHI partitioning, the BRABO package [23] was used in conjunction with the STOCK program [24].

Finally, gas-phase interaction energies were calculated for both tweezers in both angular and planar structures with sodium cation according to Eq. (4). The basis set superposition error (BSSE) was included via the counterpoise (CP) method of Boys and Bernardi [25]:

$$\Delta E_{\mathrm{int}} = E_{\mathrm{tweezer+Na^+}} - E_{\mathrm{tweezer}} - E_{\mathrm{Na^+}} \tag{4}$$

where ΔE_{int} is the interaction energy for the tweezers, $E_{\mathrm{tweezer+Na^+}}$ is the optimized energy for the tweezer and the cation, E_{tweezer} is the energy from the isolated tweezer, and $E_{\mathrm{Na^+}}$ is the energy for the sodium cation.

Molecular orbitals and geometries were plotted using the GaussView and Chemcraft visualization software [26, 27].

3 Results and discussion

The two tweezers showed an angular structure at all levels of theory due to the well-known lack of planarity of the cyclooctatetraene. In this sense, we must point out that when a constrained optimization freezing the dihedral angles is performed to obtain a planar structure, a transition state is found for both molecules. The energy differences between the conformations are shown in Tables S1 at different theoretical levels.

V-shaped and planar structures were employed as a starting geometry to perform a full optimization of the complex (with the Na cation), observing that the initial angular structure was in all cases the most stable with all functionals.

Furthermore, sodium cation distance from the tweezers was ~ 2.0 Å in both tw1 and tw2 in the virtual planar geometry, while distance in the angular geometry was ~ 3.3 Å for tw1, and ~ 2.7 Å for tw2. The influence of the DFT functional and basis set used in the calculation on the angle obtained was also analyzed. Angles measurements obtained from multilinear regression in both tweezers were investigated in both basis sets mentioned before in the computational details. Comparing the tweezers with the complexes with sodium, the angles clearly changed in tw1 than tw2 in both basis sets in all the computational levels. Both B3LYP and CAM-B3LYP showed the same change in angle values of 10.4° at the basis set of 6-31G(d,p) and 11.2° at the basis set of 6-31G(2d,2p) for tw1. The most notable change in angles was noticed at tw1 in both basis sets. The most noticeable variation when the cation is included is observed with the functional MN12L for both tweezers in both basis sets. For tw2 the change was lower than tw1 with a value of 1°–5°. The rest of the measurements are summarized in Table 1. On the other hand, Yamaguchi et al. included the dihedral angle of the nonplanar bonds in the cyclooctatetraene [5] from the X-ray structure without the sodium cation (127.2°). According to our results at 6-31G(d,p) basis set, this dihedral angle corresponds to values of 129.4°, 124.7°, 122.7°, 130.9°, 126.9° and 121.7° for B3LYP, CAM-B3LYP, M062X, MN12L, MN12SX and ωB97XD, respectively. Curiously, all these values are systematically lower than those obtained from the multilinear regression analysis, indicating an underestimation of the real molecular angle. Anyway, the closest angles with respect to the experimental one are MN12SX, B3LYP and CAM-B3LYP.

Figure 2 collects the interaction energy data calculated through Eq. 4. It is significant that the interaction is always stronger with the angular structure, being especially very powerful in the second tweezer. This is not surprising if we look at the optimized structures shown in Fig. 3. The tw2 in the angular structure closes around the cation, interacting with the entire structure. However, in tw1 and the planar structures, the interaction is reduced only to the central part.

TDDFT calculations were performed at CAM-B3LYP level with 6-31G(d,p) basis set. The first 20 excited states were considered. For tw2, different functional and basis set were employed as figure S1 shows, concluding the selection

Table 1 Angles measurements (Θ) in degrees (°) in both tw1 and tw2 at B3LYP, CAM-B3LYP, M062X, MN12L, MN12SX, and ωB97X-D, with 6-31G (d,p) and 6-31G(2d,2p) basis sets

	6-31G(d,p)				6-31G(2d,2p)			
	tw1		tw2		tw1		tw2	
	Angular	Angular + Na	Angular	Angular + Na	Angular	Angular + Na	Angular	Angular + Na
B3LYP	152.9	142.5	115.4	111.1	152.5	141.3	114.7	111.1
CAM-B3LYP	149.4	139.0	112.1	109.9	149.0	137.6	111.6	109.8
M062X	147.5	136.1	110.5	109.5	147.4	134.7	110.4	109.5
MN12L	153.8	136.9	114.4	109.7	154.6	135.5	114.6	109.8
MN12SX	150.7	138.4	113.0	109.6	150.9	136.5	112.9	109.7
ωB97XD	146.8	136.3	113.7	110.0	146.5	135.0	113.4	109.4

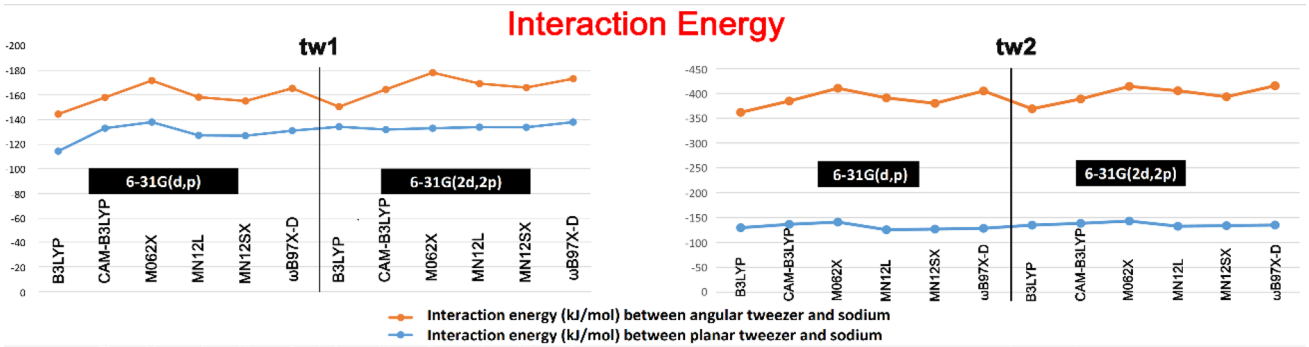

Fig. 2 The interaction energy (kJ/mol) of planar tw1 and tw2 structures and the corresponding angular molecules with sodium cation at the levels of B3LYP, CAM-B3LYP, M062X, MN12L, MN12SX, and ωB97X-D density functional theories with different Pople basis sets: 6-31G(d,p), and 6-31G(2d,2p)

of CAM-B3LYP/6-31G(d,p) as theoretical level. This DFT functional is presented as a good selection for TDDFT in different studies [28]. Table S2 summarizes the transition energies, main molecular orbitals implied and oscillator strengths (*f*) for the calculated excitations. Thanks to the computational study, we can assign the two fundamental peaks of the experimental spectrum of tw1 [5] to transits 5 and 11 (we must remember that this is approximate since our spectrum is in gas phase and the experimental in solvent). Figure 4 summarizes the UV–vis spectrum for both tweezers with and without Na cation. For tw1, the introduction of cation does not change the shape of spectrum, it only shifts the band towards a shorter wavelength. In tw2 case, the effect of the cation modifies the shape and height of the spectrum, as well as shifting towards shorter wavelengths.

Also, the greater interaction between cation and tw2 is observed at the orbital level. Thus, as shown in Fig. 5, the HOMO–LUMO gap in tw1 almost does not vary when introducing the cation, while for tw2 there is an increase in the energy difference of almost 1 eV. In Fig. 5 we can also see the shape of the HOMO and LUMO orbitals for the four systems analyzed.

The analysis of the molecular orbitals involved in the main electronic transitions is of great interest when analyzing the system's possibility of presenting important optical properties. Thus, several studies [29] have postulated the relationship between nonlinear optical responses and intramolecular charge transfer, ICT. For this reason, Figures S2 collect the molecular orbitals involved in firsts electronic transitions for both tweezers, showing that some transitions can be involved in process of ICT. As example, we observe that, for the transition of the largest oscillator strength in tw1 (286.6 nm) with 138, 140, 141 and 143 molecular orbitals involved (Table S2), the electron distribution in the occupied molecular orbitals, H-2 (138) and H (140), is mainly localized in the central part of the tweezer and moved to an external part in orbitals L (141) and L + 2 (143).

To understand the interactions between the tweezers and the cation, a QTAIM topological study was performed for both planar and angular tweezers, including sodium as well, to shed light on the nature of this non-covalent interaction. First, we analyzed the electron density critical points (CPs). We show only the results obtained at

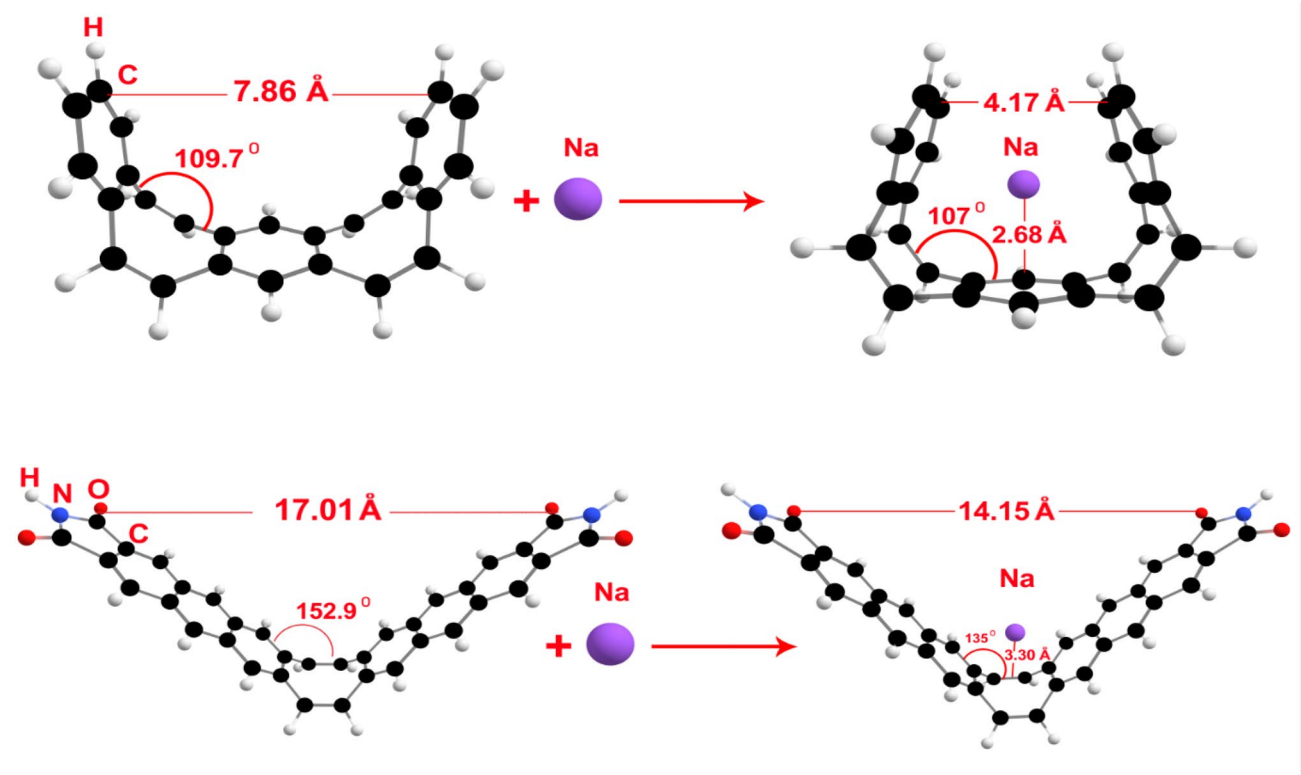

Fig. 3 Schematic representation of optimized angular geometries for tw1 (bottom), tw2 (top) and their interaction with a sodium cation. Three different parameters are presented: angle (Θ) in °, the distance between the tweezer arms in angstrom Å, and the distance between the tweezer central ring and the sodium cation in angstrom Å, at B3LYP/6-31G(d,p) level of theory

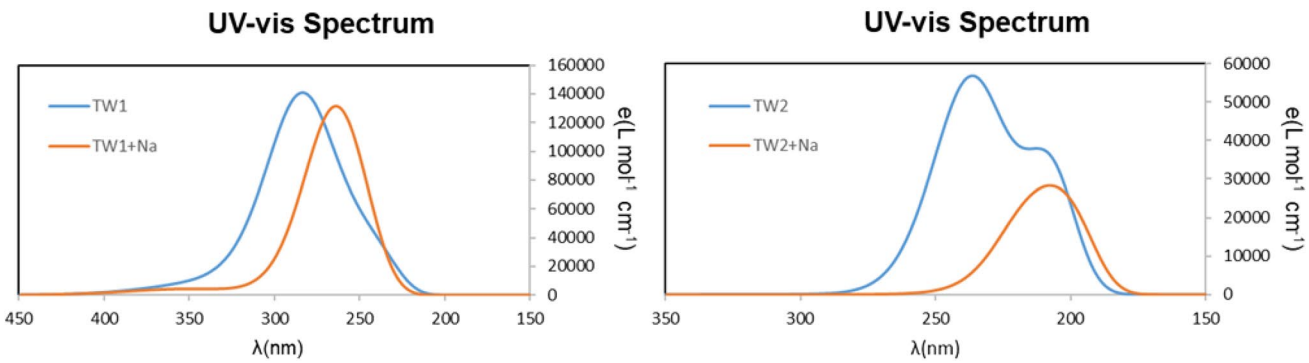

Fig. 4 UV–Vis spectrum of both tweezers with and without cation Na at CAM-B3LYP/6-31G(d,p) level

CAM-B3LYP/6-31G(d,p), since we did not find significant changes with the other functionals and the larger basis set (QTAIM calculations with all DFT functionals were performed and, as an example, the results with B3LYP, CAM-B3LYP, M062X, MN12L functionals for tw1 are shown in Tables S4). The values of the electron density computed at the ring critical points (RCPs) for tw1 and tw2 are displayed in blue in Figs. 6 and 7, respectively. In all cases, the effect of the cation in modifying the electron density of the RCPs is moderate. In turn, the cation clearly affects the ring(s) closer to the cation for tw1 (cyclooctatetraene), while all the rings for tw2 are slightly modified when the structure is V-shaped, but especially those closer to the Na once again. Therefore, the significant changes are mainly attributed to the effect of the cation–π interaction and an improved confinement and stabilization of the positive charge of the cation on the electronic structure of the tweezers.

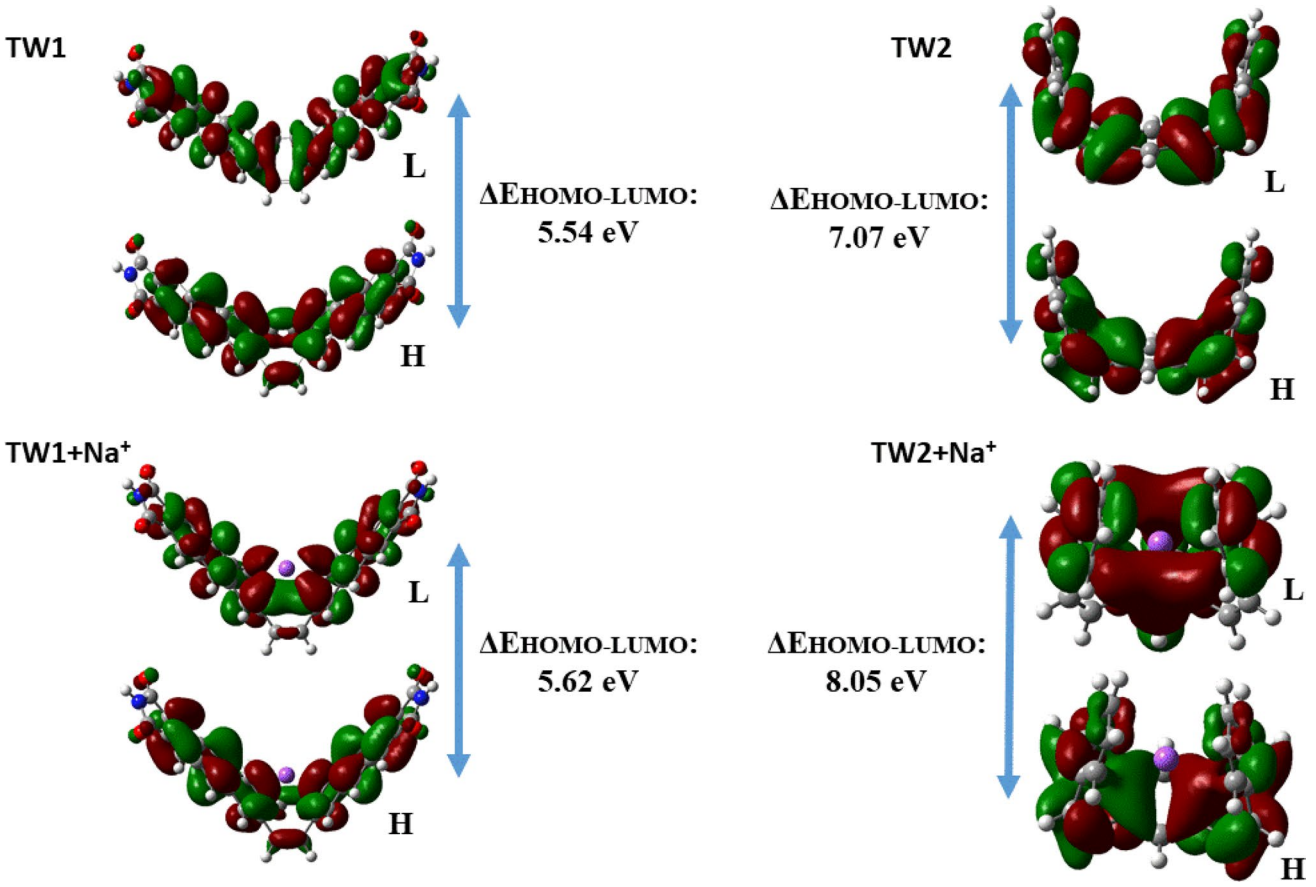

Fig. 5 HOMO and LUMO orbitals for the analyzed structures at CAM-B3LYP/6-31G(d,p) level

Regarding the bond critical points (BCPs) and the corresponding associated bond paths (BPs), sodium and tw1 are connected by two BPs, each of which seems to connect the cation to a C=C bond (Fig. 6b, d). However, the direction changes depending on the structure considered. Thereby, in the planar (angular) geometry, the bond path ends at the C1–C1' (C2) double bond and its symmetrically equivalent counterpart of the cyclooctatetraene ring. It is also worth noting the change in direction: while the bond paths in the angular tw1 follow the direction of the molecule, those of the planar counterpart follow a perpendicular direction.

When the sodium cation interacts with the planar tw2 (as shown in Fig. 7b), the corresponding BPs are directly connected to the carbon labeled C1 and its symmetrically equivalent counterpart. In contrast, in the case of tw2 + Na^+, the BPs are again attached to double bonds. In addition to the same carbons, as in the angular tw1, the alkali ion is affected by two BPs linked to double bonds from atom C5 and its symmetrically equivalent atoms. This increase in the number of BCPs leads to the appearance of several RCPs and cage critical points (CCPs) of low electron density (between 2 and 4 times less) compared to the typical RCPs observed in the benzene rings of the tweezers, as can be observed in Tables S3 in ESI. The cation tends to approach the carbon atoms with which it can form a stronger interaction, as far as its displacement within the tweezer cavity is allowed. The rest of the BPs and CPs are typical with distances and electron density values very similar to the benzene, cyclooctatetraene and pyrrolidine-2,5-dione molecules.

In Table 2, we summarize the results of some properties of the BCPs involved in the interaction between the cation and the carbons, *id est*, the atoms of the tweezer implicated in the interaction with Na through a BP. Broadly speaking, the strength of a chemical bond is related to its bond order and is manifested in the electron density at the BCP (ρ_b) [30]. Typically, in this molecule, we have observed that C–H and C–C ρ_b are between 0.24 and 0.35 au (as seen in the purple values in Figs. 6, 7). This range is far from the values observed in Table 2, where the strength is at least 10 times lower, indicating a weaker interaction than the conventional bonds forming the skeleton of both tweezers. However, it is still possible to highlight some differences between the systems. In the case of both tw1 conformers in Table 2, the two values are similar (~ 0.012 au vs. ~ 0.013 au), in striking contrast to the two tw2 conformations. On the one hand, the planar structure receives the largest value of these, implying

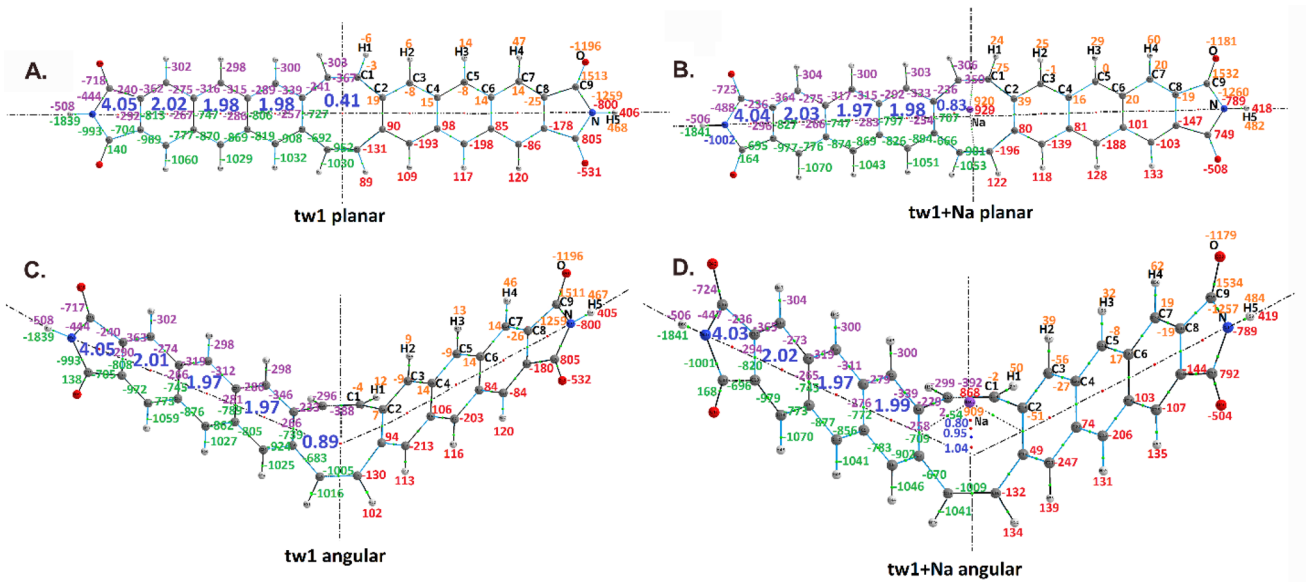

Fig. 6 Critical points, values and numbering (in black) for tweezer tw1 planar, **A** without Na cation and **B** with Na cation, and angular, **C** without Na cation and **D** with Na cation, conformations. Values in purple and green at the bond critical points (BCPs), r_b, are the Laplacian electron density $\nabla^2\rho(\mathbf{r}_b)$ and the electronic energy density, $H(r)$, respectively. Values in red and orange correspond to the FOHI and QTAIM charges, respectively. Values in blue correspond to the $\rho(\mathbf{r}_b)$ at the ring critical points (RCPs). All values are in au and multiplied by 10^3. BCPs (green dots), RCPs (red dots), and cage critical points (blue dots) were also included. All densities were obtained at CAM-B3LYP/6-31G(d,p). Vertical and horizontal lines divide the tweezers into four symmetrically equivalent regions to simplify the information provided

a direct strong interaction between C1 and Na atoms. On the other hand, the V-shaped tw2 contains four "anchors" but with weaker BCPs (considering the symmetry, we have only included two in Table 2. Curiously, the sum of both is of the same order as the two BCPs observed in the angular tw1 but slightly larger, suggesting a stronger interaction than those of the two tw1 conformers.

The Laplacian of the electron density at the BCP ($\nabla^2\rho_b$) is a useful tool for classifying bond types. In general, it can indicate whether the interaction is dominated by a covalent (shared) or ionic behavior if the values are negative or positive, respectively [30, 31]. The negative sign represents an accumulation of electron density on the BCP along the bond path, while values greater than zero denote a depletion of electron density on the BCP toward each nucleus, provoking a closed-shell (ionic) interaction. For example, all C–C and C–H BCPs are less than zero (as seen in Table S7 in the ESI), revealing that these atoms share electrons, while all C–Na^+ BCPs in Table 2 are clearly positive. This suggests a closed-shell systems interaction, typical of ionic bonds or cation–π interactions. To obtain more information about the nature of the interaction, the value of $\nabla^2\rho_b$ can be decomposed by the local virial theorem [28] into two terms at the BCP, r_b, namely the gradient kinetic energy density ($G(\mathbf{r}_b)$), which shows the tendency of the system to escape electrons from r_b, and the virial field or potential energy density ($V(\mathbf{r}_b)$), which represents the ability of the system to accumulate electrons at r_b [31]:

$$2G(r_b) + V(r_b) = \frac{1}{4}\nabla^2\rho_b \tag{5}$$

This expression is defined in au. If we divide it by $-G(\mathbf{r}_b)$ and change the second term to the second member of Eq. 5, we obtain the following expression:

$$-\frac{V(r_b)}{G(r_b)} = -\frac{\nabla^2\rho_b}{4G(r_b)} + 2 \tag{6}$$

The value of minus the fraction in the first member of Eq. 6 is positive and depends on the sign of the Laplacian, since the virial field and the gradient kinetic energy density are negative and positive, respectively. If $\nabla^2\rho_b$ is positive (negative), the fraction $-V(\mathbf{r}_b)/G(\mathbf{r}_b)$ is less (greater) than 2 and reflects an ionic or noncovalent (covalent) behavior, since $G(\mathbf{r}_b)$ ($V(\mathbf{r}_b)$) dominates, and the system prefers to avoid (accumulate) electrons on the BCP. In parallel, the sum of $G(\mathbf{r}_b)$ and $V(\mathbf{r}_b)$, namely the total energy density, $H(\mathbf{r}_b)$, is sometimes combined with this ratio to study the type of interaction formed. However, covalent or closed-shell behavior is not absolute, so Espinosa et al. [32] defined a scale consisting of three regions: Region (I) for pure closed-shell interactions whether $\left|V(r_b)\right| < G(r_b)$| or

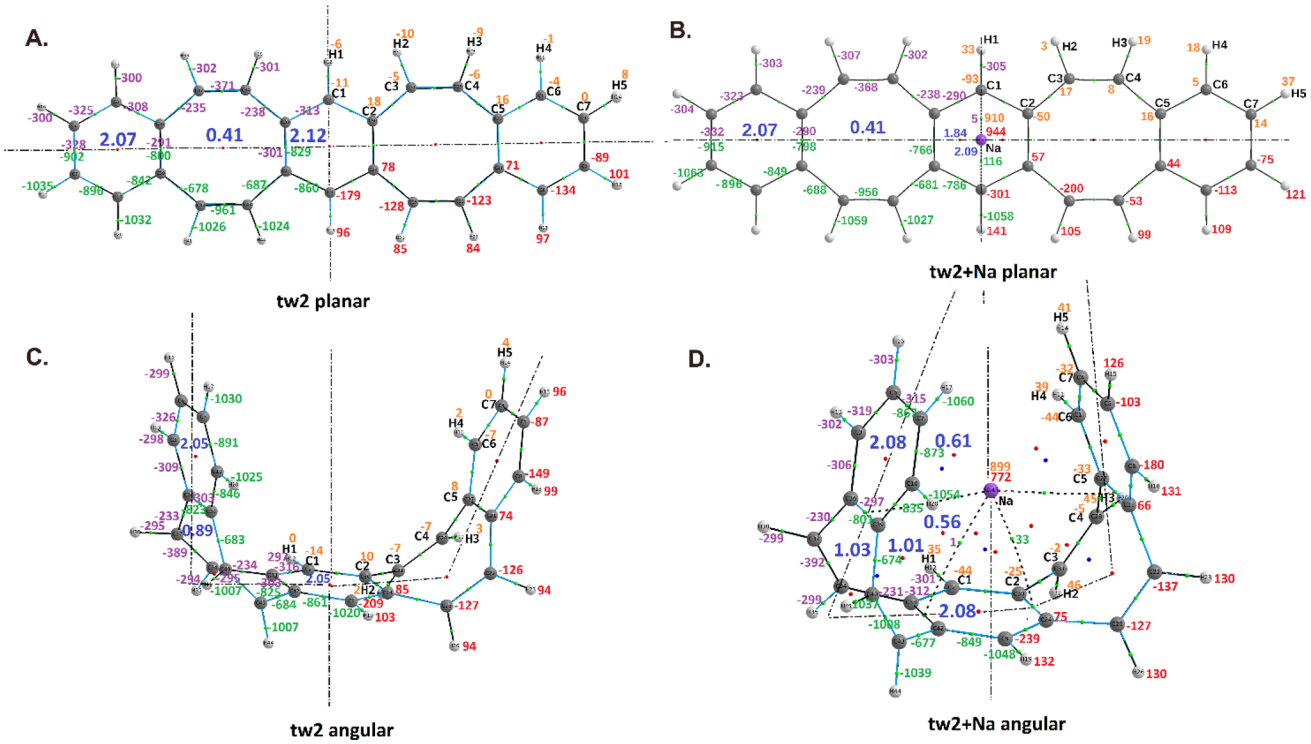

Fig. 7 Critical points, values and numbering (in black) for tweezer tw2 planar, **A** without Na cation and **B** with Na cation, and angular, **C** without Na cation and **D** with Na cation, conformations. Values in purple and green at the bond critical points (BCPs), $\boldsymbol{r}_b$, are the Laplacian electron density $\nabla^2\rho(\mathbf{r}_b)$ and the electronic energy density, $H(r)$, respectively. Values in red and orange correspond to the FOHI and QTAIM charges, respectively. Values in blue correspond to the $\rho(\mathbf{r}_b)$ at the ring critical points (RCPs). All values are in au and multiplied by 10^3. BCPs (green dots), RCPs (red dots), and cage critical points (blue dots) were also included. All densities were obtained at CAM-B3LYP/6-31G(d,p). Vertical and horizontal lines divide the tweezers into four symmetrically equivalent regions to simplify the information provided

Table 2 Implied carbons with one of their bond paths ending at the sodium cation together with the values of the following topological properties at the involved bond critical points (BCPs), $\boldsymbol{r}_b$: electron density ρ_b, Laplacian of the electron density $\nabla^2\rho_b$, virial field $V(\boldsymbol{r}_b)$, gradient kinetic density $G(\boldsymbol{r}_b)$, the ratio of $-V(\boldsymbol{r}_b)/G(\boldsymbol{r}_b)$ for both tweezers in the angular and planar geometry, and total energy density $H(\boldsymbol{r}_b)$

Tweezers	Bond	ρ_b	$\nabla^2\rho_b$	$V(r_b)$	$G(r_b)$	$-V(r_b)/G(r_b)$	$H(r_b)$
Angular tw1 + Na	C2···Na	11.75	53.64	−9.15	11.28	0.81	2.13
Planar tw1 + Na	C1···Na	13.03	59.24	−9.95	12.38	0.80	2.43
Angular tw2 + Na	C2···Na	6.11	25.44	−4.58	5.47	0.84	0.89
Angular tw2 + Na	C5···Na	7.73	32.56	−5.84	6.99	0.84	1.15
Planar tw2 + Na	C1···Na	20.69	115.64	−19.65	24.28	0.81	4.63

All electron densities were computed at CAM-B3LYP/6-31G(d,p). All values except $-V(\boldsymbol{r}_b)/G(\boldsymbol{r}_b)$ are in au and multiplied by 10^3

$H(r_b) > 0$, region (II) for intermediate closed-shell behavior whether $G(r_b) < |V(r_b)| < 2G(r_b)$ or $-G(r_b) < H(r_b) < 0$, and region (III) for shared-shell character, where $|V(r_b)| > 2G(r_b)$ or $H(r_b) < -G(r_b)$. According to Table 2, the values of this ratio are clearly less than one for all the tweezers studied, which means that the type of interaction between the sodium cation and all the tweezers points to a closed-shell behavior. The same observation is certainly true for the total energy density, since all values are greater than zero, even though this long-range interaction is not as strong as that of a typical ionic bond according to the small value obtained. For comparison, we have included the values of $H(\boldsymbol{r}_b)$ (in green) for the rest of the

bonds in Figs. 6 and 7. As can be seen, they are of opposite sign and much stronger than those of C–Na.

The previous topological parameters do not provide a readily illustrative tool for analyzing the changes induced by the inclusion of the alkali cation, i.e., they do not give an intuitive idea of which atoms or groups of atoms are mainly involved in the distribution of the positive charge coming from the Na cation. Nevertheless, the QTAIM approach also provides a very useful method for partitioning the molecular space into discrete mononuclear regions identified as atoms. The QTAIM atom definition, with solid and natural foundations, assumes that the boundaries of an atom depend on the surfaces of zero flux in the gradient vector field of the electron density. This partitioning strategy is also compared to another atomic partitioning based on the Hirshfeld idea (Eq. 3), where the concept of atom emerges from fuzzy regions defined by a weight function [33]. The way the molecular space is separated is completely different for both methods, but together they can provide more insight from different points of view.

We will look at both tweezers without the Na cation. Three types of carbon can be observed, as shown in Figs. 6 and 7. First, those in tw1 (Fig. 6) around the oxygen and nitrogen atoms are strongly charged in both partitionings, even though we will discuss this below. Second, the bridging carbons that are bonded to other C atoms are positively charged (except for C8 in tw1 due to a mesomeric effect). Third, the carbons bonded to the hydrogens (C1, C3 and C5 in tw1, C1, C3, C4, C6 and C7 in tw2, Fig. 7), whose charge is null or slightly negative in the case of QTAIM and, on the contrary, more than −0.122 au when the FOHI scheme is considered. These charges seem to be against the latter partitioning. However, considering the Pauling electronegativity scale, where $\chi(O) = 3.44 > \chi(N) = 3.04 > \chi(C) = 2.55 > \chi(H) = 2.2$, the difference between C and H is large enough to observe this type of electron donation from H atoms. In addition, the carbon atoms are relatively confined in the QTAIM basin compared to the entire molecular space considered in Hirshfeld-based schemes. In any case, the QTAIM basins of these atoms recover the six electrons of the carbon, implying that the FOHI negative charge seems to be caused by the p_z delocalization. On the contrary, the bridge carbons (C2, C4 and C6 in tw1, and C2 and C5 in tw2) are positively charged in both partitionings. Again, the FOHI values are larger in absolute value than those from the QTAIM partitioning. Finally, the carbon atoms near the oxygen and nitrogen atoms in tw1 are affected by the strong electronegativity difference. In fact, they are very negatively charged ($q(O) = -1.196$ au and $q(N) = -1.259$ au for the QTAIM partitioning, $q(O) \simeq -0.530$ au and $q(N) = -0.800$ au for the FOHI partitioning), even though this charge effect is more mitigated in the case of the Hirshfeld-based partitioning scheme. Due to these strong charges coming from O and N atoms, C9, the atom in α, presents a large electron deficit, with 1.510 and 0.805 electrons less for QTAIM and FOHI, respectively. In contrast, C8, the atom in β with respect to the O and N atoms, increases its electron population affected by a mesomeric effect coming from C9, N and O atoms as was observed previously in the indole [31], where the bridging carbon was also negatively charged due to a π-donation in view of the QTAIM analysis at B3LYP/6-311++G(2d,2p) (6.007 au and 1.029 au for the total and π populations, respectively). However, a more detailed study focusing on σ/π populations and 2-delocalization indices to investigate this effect is beyond the scope of this work.

Regarding the hydrogen atoms, as already mentioned, some differences can be observed between the two partitioning schemes. On the one hand, the QTAIM approach keeps the hydrogens slightly charged (H1–H3 and H1–H5 in tw1 in Fig. 6 and in tw2 in Fig. 7, respectively) with values less than 0.015 au in absolute value. However, the hydrogens in tw1 are positively charged (except for H1 in the planar structure) in contrast to tw2 where they are negatively charged. On the other hand, the FOHI hydrogen charges are always positive in any case (between + 0.084 au and + 0.120 au for the hydrogens mentioned above), strictly following the widely accepted electronegativity scale. H4 and H5 in tw1 are a special case, since the former is close to and influenced by the O atom, and the latter is bonded to the N atom, the most negatively charged atom in the molecule, and loses between 0.405 and 0.468 electrons.

When the sodium cation interacts with the tweezers, more than 75% of its initial charge (+ 1 au) is retained in the alkali atom for both tw1 (Fig. 6) and tw2 (Fig. 7). The largest values are observed in the case of the planar structures where the alkali atom uniquely has a ring close to polarize the π electrons, either cyclooctatetraene (tw1) or benzene (tw2), and the charge is recovered at 92.0–92.9% and 91.0–94.4% for tw1 and tw2, respectively. Curiously, planar tw1 provides a very similar QTAIM and FOHI Na charge (+ 0.920 vs + 0.929, respectively), but tw2 presents a relatively important difference, 0.084 au in favor of the QTAIM approach (Na is less charged). Conversely, both angular structures, and especially tw2, counteract the positive charge better because more rings (and therefore more available π electrons) are implied in the interaction with Na. Thus, the alkali atom recovers the 90.9% and 86.8% in tw1, and 89.9% and 77.2% in tw2 for the QTAIM and FOHI splitting, respectively. In this case, the FOHI scheme recovers less than the QTAIM approach, probably due to the difference between the whole molecular space considered with the FOHI partitioning, which gives the opportunity to take more electron density to counteract the positive charge of the sodium than the confined QTAIM basin. The loss of electron density induced by the Na cation reorganizes the charges of both tweezers in the two conformations. By

Table 3 QTAIM and FOHI relative populations (ΔN) of both tw1 and tw2 tweezers bonded to the sodium cation with respect to the isolated tweezers

Atoms	tw1				tw2			
	QTAIM		FOHI		QTAIM		FOHI	
	ΔN P + Na	ΔN A + Na	ΔN P + Na	ΔN A + Na	ΔN P + Na	ΔN A + Na	ΔN P + Na	ΔN A + Na
C1	72	−2	65	2	82	30	122	30
C2	−20	58	10	45	68	35	21	10
C3	−7	47	−54	34	−22	−5	72	0
C4	−1	41	17	32	−14	−2	−70	11
C5	−8	−1	−10	3	0	41	27	8
C6	−6	−3	−16	−19	−9	48	−21	31
C7	−6	−5	17	23	−14	32	−14	16
C8	−6	−7	−31	−36				
C9	−19	−23	56	13				
$\sum\Delta N$(H)	−91	−120	−78	−102	−128	−195	−112	−163
O	−15	−17	−23	−28				
N	1	−2	−11	−11				

P and A denote planar and angular conformations, respectively. $\sum\Delta N$(H) represents the sum of all hydrogen atoms, taking symmetry into account. The carbons used in this table follow the numbering from Figs. 6 and 7. All values are in au and multiplied by 10^3

and large, the atoms most affected are the hydrogens, whose population decreases (they are more positively charged), as can be observed in Table 3, where we have included the sum of the population variations of these atoms ($\sum\Delta N$(H)) caused by Na^+. In this way, H atoms lose between 0.078 au (FOHI value for planar tw1) and 0.195 au (QTAIM value for angular tw2), where the sign indicates the depletion. Furthermore, in both partitioning schemes we observe an important difference between the electron donation from the hydrogens associated with the charge transfer to the sodium cation. The more the hydrogens are depleted, the lower the Na population is in Figs. 6B, D and 7B, D. Peculiarly, the same lessening effect happens with the oxygen atom in tw1, i.e., the negative charge decreases by 0.015 au and 0.023 au (0.017 au and 0.028 au) for the planar (angular) structure for QTAIM and FOHI charges, respectively. In the case of the nitrogen, however, the effect is smaller for FOHI charges ($\Delta q = 0.012$ au) and virtually zero for QTAIM.

In Table 3, we have collected all the relative populations (ΔN) for all the carbon atoms of tw1 and tw2 interacting with the sodium cation with respect to the isolated molecule. The positive charge coming from the alkali cation attracts the electron density towards the atoms closer to this atom, causing a general depletion of the hydrogen populations, as mentioned before, in view of the electron conservation. This affects the carbons skeleton in various ways. For example, electron shifts provoke several carbon atoms to gain electron density despite the positive Na charge, especially C1 in planar tw1, C2 in angular tw1, and C1 and C2 in tw2. This effect is particularly evident in explaining the bond paths that follow the maximum electron density observed in Figs. 6B, D and 7B, D. In the case of planar tw1, C1 increases its population (i.e., it is more negatively charged), and the BP ends in the middle of the C1–C1' bond. On the other hand, in the V-shaped structure, C2 is the atom whose electron density increases more (0.058 au and 0.045 au for QTAIM and FOHI schemes, respectively), and the BP ends in the corresponding bond associated with this atom. However, this is more difficult to distinguish for tw2, where C1 and C2 clearly grow their populations, especially C1 for the planar structure, but the behavior of these atoms in the V-shaped structure is more erratic, with some discrepancies with both partitionings, produced by the four BPs found (Fig. 7D) that share the Na stabilization. In fact, positive variations with the QTAIM approach are observed in two more carbons, C5 and C6, as predicted by the BPs. The FOHI partitioning does not follow the same trend, probably because the grid integration considers the whole molecular space instead of the discrete QTAIM basins. In the planar tw1, the same happens with C3-C8, i.e., while the planar structure presents virtually zero ΔN (< 0.009 au) with the QTAIM approach, the FOHI results are larger in absolute value and C4 and C7 increase their relative population. Strangely, these carbon atoms represent different environments. Thus, C4 is a bridging atom bonded to three carbon atoms, while C7 is one of the atoms bonded to hydrogens and in γ position to the O and N atoms (probably affected by resonance effects). A very similar situation is repeated with the angular tw1, but from C5 to C8, because C3 and C4 are closer to the sodium cation than the atoms in the planar conformation and they clearly enlarge their population in both partitionings.

In the case of tw2, the effect from C3 to C7 atoms is more atypical. The planar structure loses population at C3 and C4 with the QTAIM approach, while the FOHI scheme shows a different trend, with a significant population increase (decrease) at C3 (C4), since ΔN is greater (less) than zero. Moreover, C5 is unchanged in the QTAIM approach in contrast to the FOHI relative populations, where the value grows. C6 and C7 suffer from electron depletion in both partitionings. On the contrary, the V-shaped tw2 carbons are significantly different. They are closer to the sodium atom and the partial positive charge of the Na causes population accumulation in all atoms except C3 and C4, where the population is slightly modified.

4 Conclusions

A structural, energetic, orbital and topological analysis of two promising molecules to use as tweezers or in optoelectronic applications were performed. Calculations were carried out with different DFT functional and two basis sets. The formation of complex with Na cation were also considered.

This extensive computational study allows us to verify the potential of the systems analyzed, presenting itself as introductory since it opens new paths of study that we intend to carry out. Thus, on the one hand, we consider necessary an in-depth study of the excited states that would allow us to present the potential of these systems in optoelectronic applications. On the other hand, we propose to carry out dynamic studies of the complexation processes with cations or other systems.

Nevertheless, the analysis allows us to conclude important data such as: the preference of the systems for the angular structure, being, in both systems and for all the levels of calculation used, the flat structure a transition state in the ground state.

Quantum Theory of Atoms In Molecules (QTAIM) topology analysis of the electron density clearly indicates a closed shell interaction between the sodium cation and both tweezers. Population analysis, carried out using QTAIM partitioning and a Hirshfeld-based atomic scheme called Fractional Occupation Hirshfeld-I, indicates a small charge transfer from the tweezers to the sodium cation, between 0.034 and 0.250 au, depending on whether these molecules are open or closed, anchored to the cation. Most of these electron distributions come from the hydrogen atoms in both partitioning schemes. The cation causes an increase in the electron populations of the closer atoms whose bonding paths end in the alkali atom.

It is also interesting to note that complexation leads to a major modification on the UV–Vis spectrum for tw2.

In summary, tw1 and tw2 are presented as systems of great interest and new studies are proposed for their use as tweezers, in molecular electronics, sensing or optical applications.

Supplementary Information The online version contains supplementary material available at https://doi.org/10.1007/s00214-023-03038-0.

Acknowledgements We acknowledge the financial support by Xunta de Galicia (GRC2019/24) and the funding for open access charge by Universidade de Vigo/CISUG. N. Otero thanks the University of Vigo for the postdoctoral grant within the "Retención de Talento Investigador da Universidade de Vigo 2020".

Author contributions MS, NO and APG wrote the main manuscript text. NO and APG reviewed the manuscript.

Funding Open Access funding provided thanks to the CRUE-CSIC agreement with Springer Nature.

Declarations

Conflict of interests The authors declare no competing interests.

References

1. Li J, Terec A, Wang Y, Joshi H, Lu Y, Sun H, Stuparu MC (2017) J Am Chem Soc 139:3089
2. Nishinaga T, Ohmae T, Iyoda M (2010) Symmetry 2:76
3. Stępień M, Sprutta N, Latos-Grazyński L (2011) Angew Chem Int Ed 50:4288
4. Würthner F (2006) Pure Appl Chem 78:2341
5. Yuan C, Saito S, Camacho C, Irle S, Hisaki I, Yamaguchi S (2013) J Am Chem Soc 135:8842
6. Chen CW, Whitlock HW (1978) J Am Chem Soc 100:4921
7. Nishiuchi T, Iyoda M (2015) Chem Rec 15:329
8. Nishiuchi T, Iyoda M (2014) Bull Chem Soc Jpn 87:960
9. Tirado-Rives J, Jorgensen WL (2008) J Chem Theory Comput 4:297
10. Yanai T, Tew DP, Handy NC (2004) Chem Phys Lett 393:51
11. Zhao Y, Truhlar DG (2008) Theor Chem Acc 120:215
12. Peverati R, Truhlar DG (2012) Phys Chem Chem Phys 14:13171
13. Peverati R, Truhlar DG (2012) Phys Chem Chem Phys 14:16187
14. Chai JD, Head-Gordon M (2008) Phys Chem Chem Phys 10:6615
15. Frisch MJ, Trucks GW, Schlegel HB, Scuseria GE, Robb MA, Cheeseman JR, Scalmani G, Barone V, Petersson GA, Nakatsuji H, Li X, Caricato M, Marenich A V, Bloino J, Janesko BG, Gomperts R, Mennucci B, Hratchian HP, Ortiz J V, Izmaylov AF, Sonnenberg JL, Williams-Young D, Ding F, Lipparini F, Egidi F, Goings J, Peng B, Petrone A, Henderson T, Ranasinghe D, Zakrzewski VG, Gao J, Rega N, Zheng G, Liang W, Hada M,

Ehara M, Toyota K, Fukuda R, Hasegawa J, Ishida M, Nakajima T, Honda Y, Kitao O, Nakai H, Vreven T, Throssell K, Montgomery Jr. JA, Peralta JE, Ogliaro F, Bearpark MJ, Heyd JJ, Brothers EN, Kudin KN, Staroverov VN, Keith TA, Kobayashi R, Normand J, Raghavachari K, Rendell AP, Burant JC, Iyengar SS, Tomasi J, Cossi M, Millam JM, Klene M, Adamo C, Cammi R, Ochterski JW, Martin RL, Morokuma K, Farkas O, Foresman JB, Fox DJ (2009) Gaussian 09 Revision A.02

16. Trani F, Scalmani G, Zheng G, Carnimeo I, Frisch MJ, Barone V (2011) J Chem Theory Comput 7:3304
17. Gąsiorski P, Danel KS, Matusiewicz M, Uchacz T, Kuźnik W, Kityk A V (2012) J Fluoresc 22:81
18. Gąsiorski P, Danel KS, Matusiewicz M, Uchacz T, Kuźnik W, Piatek Ł, Kityk A V (2012) Mater Chem Phys 132:330
19. Frisch MJ, Trucks GW, Schlegel HB, Scuseria GE, Robb MA, Cheeseman JR, Scalmani G, Barone V, Petersson GA, Nakatsuji H, Li X, Caricato M, Marenich A V, Bloino J, Janesko BG, Gomperts R, Mennucci B, Hratchian HP, Ortiz J V, Izmaylov AF, Sonnenberg JL, Williams-Young D, Ding F, Lipparini F, Egidi F, Goings J, Peng B, Petrone A, Henderson T, Ranasinghe D, Zakrzewski VG, Gao J, Rega N, Zheng G, Liang W, Hada M, Ehara M, Toyota K, Fukuda R, Hasegawa J, Ishida M, Nakajima T, Honda Y, Kitao O, Nakai H, Vreven T, Throssell K, Montgomery Jr. JA, Peralta JE, Ogliaro F, Bearpark MJ, Heyd JJ, Brothers EN, Kudin KN, Staroverov VN, Keith TA, Kobayashi R, Normand J, Raghavachari K, Rendell AP, Burant JC, Iyengar SS, Tomasi J, Cossi M, Millam JM, Klene M, Adamo C, Cammi R, Ochterski JW, Martin RL, Morokuma K, Farkas O, Foresman JB, Fox DJ (2016) Gaussian˜16 Revision C.01
20. Bader RFW (1991) A quantum theory of molecular structure and its applications. Chem Rev 91:893
21. Geldof D, Krishtal A, Blockhuys F, Van Alsenoy C (2011) J Chem Theory Comput 7:1328
22. Keith TA (2019) AIMAll (Version 19.10.12), TK Gristmill Software, Overland Park KS, USA. http://aim.tkgristmill.com. Accessed 23 May 2023
23. Van Alsenoy C, Peeters A (1993) THEOCHEM 286:19
24. Rousseau B, Peeters A, Van Alsenoy C (2000) Chem Phys Lett 324:189
25. Boys SF, Bernardi F (2002) Mol Phys 100:65
26. Chemcraft - graphical software for visualization of quantum chemistry computations. Version 1.8, build 126. https://www.chemcraftprog.com. Accessed 23 May 2023
27. Dennington R, Keith T, Milam JM, Gauss View, Version 5.0 (2009) Semichem Inc, Shawnee Mission KS
28. Laurent AD, Jacquemin D (2013) Int J Quantum Chem 113:2019
29. Ozcelik A, Pereira-Cameselle R, Peña-Gallego A, Alonso-Gómez JL (2022) Eur J Org Chem e202101333
30. Matta CF, Boyd RJ (2007) The quantum theory of atoms in molecules: from solid state to DNA and drug design. Wiley, Weinheim
31. Espinosa E, Molins E, Lecomte C (1998) Chem Phys Lett 285:170
32. Espinosa E, Alkorta I, Elguero J, Molins E (2002) J Chem Phys 117:5529
33. Otero N, González Moa MJ, Mandado M, Mosquera RA (2006) Chem Phys Lett 428:249